Journal of Marine Systems 170 (2017) 31–41

Contents lists available at ScienceDirect

Journal of Marine Systems

journal homepage: www.elsevier.com/locate/jmarsys

Sediment resuspension and the generation of intermediate nepheloid layers by shoaling internal bores

Eiji Masunaga [a,b,*], Robert S. Arthur [c], Oliver B. Fringer [d], Hidekatsu Yamazaki [b]

[a] Center for Water Environment Studies, Ibaraki University, Ibaraki, Japan
[b] Department of Ocean Sciences, Tokyo University of Marine Science and Technology, Tokyo, Japan
[c] Department of Civil and Environmental Engineering, University of California, Berkeley, CA, USA
[d] Department of Civil and Environmental Engineering, Stanford University, Stanford, CA, USA

ARTICLE INFO

Article history:
Received 24 June 2016
Received in revised form 23 January 2017
Accepted 23 January 2017
Available online 12 February 2017

Keywords:
Intermediate nepheloid layers
Sediment resuspension
Internal bores
Internal waves
Numerical simulations

ABSTRACT

Numerical simulations of sediment resuspension due to shoaling internal bores are performed with a nonhydrostatic model, SUNTANS. Results show strong sediment resuspension induced by internal bores and a turbidity layer intruding offshore in the interior of the water column, known as an intermediate nepheloid layer (INL). Sediment resuspension processes and INLs reproduced in the model are in good agreement with observational data from Otuschi Bay, Japan. The formation of INLs by shoaling internal waves is explained as follows: (1) strong receding currents due to a previous run-up bore cause sediment resuspension along the slope, (2) the interaction of the receding currents and a subsequent run-up bore induce horizontal flow convergence and strong upward currents, (3) the upward currents lift the suspended sediments into the interior of the water column, (4) the run-up bore intrudes below the suspended sediments and forms an INL within the pycnocline. Sediment resuspension processes are also investigated for various internal Iribarren number conditions. The internal Iribarren number represents the ratio of the topographic slope to the internal wave steepness. In low internal Iribarren number conditions, strong currents near the bottom result in sediment resuspension and INL formation. In high internal Iribarren number conditions, sediment resuspension is weak, and INLs do not form.

1. Introduction

The coastal ocean is generally known as a region of high biological productivity due to the presence of sediments, nutrients and organic materials. These materials can be transported by tidal flows, geostrophic flows, strong winds, surface waves, or internal waves. Typically, water with highly concentrated suspended sediments (high turbidity) exists near the sea surface and in bottom boundary layers. High turbidity surface water is usually formed by buoyant low salinity water from rivers, while high turbidity bottom water is created by downslope turbidity currents and sediment resuspension. Such high turbidity water can contain elevated levels of iron, helping maintaining ocean ecosystems (Bruland et al., 2001). In addition to near-surface and bottom high-turbidity water, numerous field surveys have reported suspended sediment layers in the interior of the water column, known as intermediate nepheloid layers (INLs) (Moum et al., 2002; McPhee-Shaw, 2006; Masunaga et al., 2015). One of the primary mechanisms generating INLs on coastal slopes is locally enhanced turbulent mixing in the bottom boundary layer. Phillips et al. (1986) and Garrett (1990) reported that locally enhanced mixing and re-stratification on the slope causes a convergent flow on the slope leading to an outflow into the ocean interior. This convergent flow is called a "tertiary" circulation (Garrett, 1990, 1991).

Internal wave breaking is known as a major contributor to boundary-layer mixing on sloping bottoms (e.g., Richards et al., 2013; Masunaga et al., 2016), and thus to the formation of INLs. Reflections of linear internal tides generate energy convergence and locally intensified currents along the slope where the incident wave angle matches the angle of the bathymetric slope (Cacchione et al., 2002; Van Gastel et al., 2009). The reflection of internal tides also leads to shoaling internal waves propagating into shallow areas. Such highly-nonlinear internal waves are often referred to as "internal bores" or "internal boluses" (e.g., Helfrich, 1992; Leichter et al., 1996; Walter et al., 2012; Masunaga et al., 2016). Internal bores induce strong currents and turbulent mixing in both the interior and the bottom boundary layer (Venayagamoorthy and Fringer, 2006; Van Haren, 2009; Walter et al., 2012; Masunaga et al., 2016). Strong sediment resuspension and the presence of INLs has also been observed during the passage of internal bores on slopes in the field

* Corresponding author at: Center for Water Environment Studies, Ibaraki University, 4-12-1, Nakanarusawa, Hitachi, Ibaraki, Japan.
E-mail address: eiji.masunaga.office@vc.ibaraki.ac.jp (E. Masunaga).

http://dx.doi.org/10.1016/j.jmarsys.2017.01.017
0924-7963/

(e.g., Van Haren, 2009; Masunaga et al., 2015) and in numerical models (e.g., Bourgault et al., 2014; Olsthoorn and Stastna, 2014; Arthur and Fringer, 2016).

Recent studies conducted by Tohoku Ecosystem-Associated Marine Sciences (TEAMS) revealed strong turbulent mixing and sediment resuspension induced by nonlinear internal bores in Otsuchi Bay located on the Sanriku Coast, Japan (e.g., Masunaga et al., 2015; Masunaga et al., 2016). The Sanriku Coast consists of numerous bays created by the partial submergence of river valleys (Fig. 1a–c). Masunaga et al. (2015) observed highly-nonlinear internal bores accompanied by INLs in Otsuchi Bay. The internal bores induce a vortex motion at the head of the bore that lifts sediments as much as 8 m above the bottom. The suspended sediments intrude into the internal wave's interface, forming INLs. Internal bores in Otsuchi Bay occur at roughly semidiurnal periods. However, their timing is not consistent with sea surface tidal elevations. The reason for this inconsistency is that background geophysical flows and stratification conditions modulate the phase speed of the internal bores. Following Masunaga et al. (2015), Masunaga et al. (2016) extended the observation area and found strong turbulent mixing induced by an interaction of a receding bore and a subsequent run-up bore, with the rate of turbulent kinetic energy dissipation reaching $O(10^{-5})$ W kg^{-1}. In addition, Masunaga et al. (2015, 2016) developed a two-dimensional numerical model that reproduced basic features of the internal bores in the bay.

Previous studies revealed strong sediment resuspension, INLs and turbulent mixing associated with internal bores in Otsuchi Bay. However, details of INL formation processes are not fully understood. To further investigate the generation of INLs by shoaling internal bores, we conduct numerical experiments using a fully non-hydrostatic and nonlinear numerical model, the Stanford Unstructured Nonhydrostatic Terrain-following Adaptive Navier-Stokes Simulator (SUNTANS, Fringer et al., 2006). Several previous studies have used SUNTANS to investigate the breaking mechanism of internal waves in shallow water (Walter et al., 2012; Masunaga et al., 2015; Masunaga et al., 2016). Here, using a similar approach to these studies, we employ two-dimensional SUNTANS simulations to examine sediment resuspension and the formation of INLs due to shoaling internal bores. Section 2 describes the model configuration. Section 3 describes sediment resuspension and INL formation due to shoaling internal bores. Section 4 presents sediment resuspension by internal bores under various bathymetric slope conditions. The last section discusses new findings from this study with major conclusions.

2. Numerical setup

2.1. Governing equations

In order to simplify the numerical computations, we employ a two-dimensional (x–z) version of SUNTANS to simulate internal wave generation and breaking processes. SUNTANS solves the Reynolds averaged Navier-Stokes equations with the Boussinesq approximation,

$$\frac{\partial \mathbf{u}}{\partial t} + \mathbf{u}\cdot\nabla\mathbf{u} = -\frac{1}{\rho_0}\nabla\rho - \frac{g}{\rho_0}\rho\vec{k} + \nabla_H\cdot(\nu_H\nabla_H\mathbf{u}) + \frac{\partial}{\partial z}\left(\nu_V\frac{\partial \mathbf{u}}{\partial z}\right) \quad (1)$$

where $\mathbf{u}$ is the velocity vector, ν is the eddy viscosity, and subscripts H and V denote the horizontal and the vertical components of a variable or operator. Because the model is two-dimensional, the Coriolis force was not included in the momentum equation. Temperature and salinity transport equations and the continuity equations are defined as

$$\frac{\partial T}{\partial t} + \nabla\cdot(\mathbf{u}T) = \nabla_H\cdot(\kappa_H\nabla_H T) + \frac{\partial}{\partial z}\left(\kappa_V\frac{\partial T}{\partial z}\right) \quad (2)$$

$$\frac{\partial S}{\partial t} + \nabla\cdot(\mathbf{u}S) = \nabla_H\cdot(\kappa_H\nabla_H S) + \frac{\partial}{\partial z}\left(\kappa_V\frac{\partial S}{\partial z}\right) \quad (3)$$

$$\nabla\cdot\mathbf{u} = 0 \quad (4)$$

where κ is the eddy diffusivity. The density is computed from temperature, salinity and pressure using the equation of state defined by Millero and Poisson (1981). In this study, the Mellor and Yamada level 2.5 turbulent closure model (Mellor and Yamada, 1982) was used to calculate the eddy-viscosity and eddy-diffusivity. Although a three-dimensional

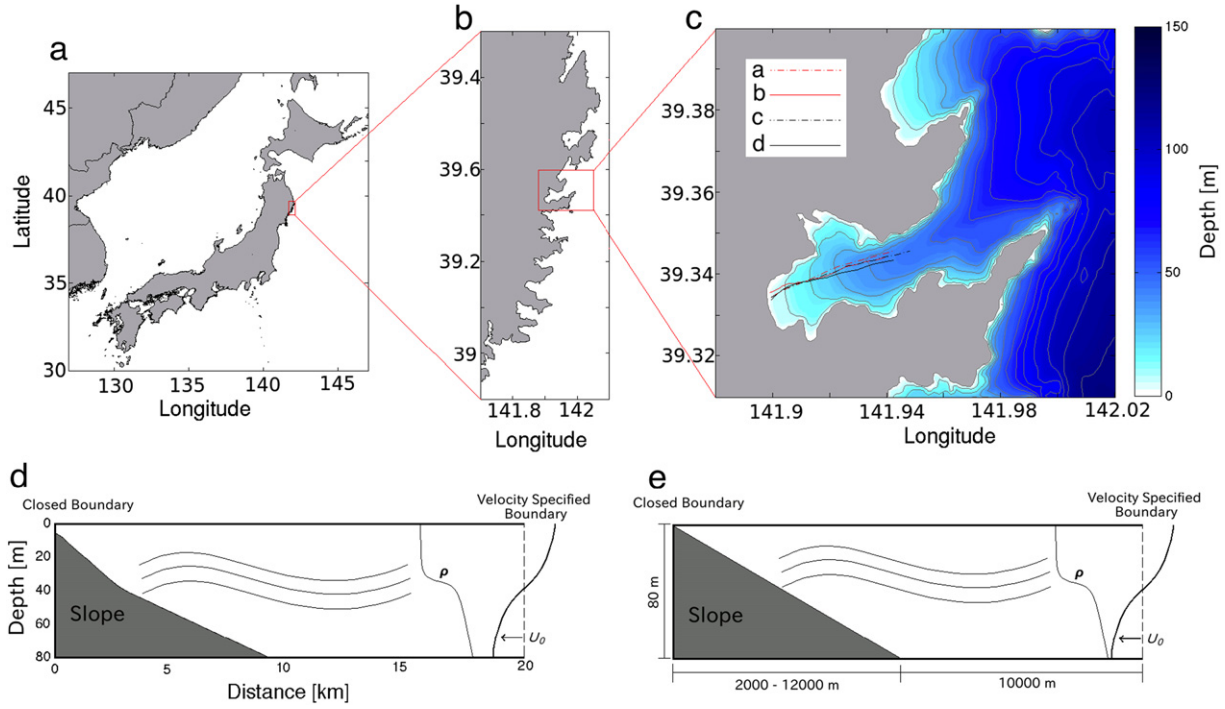

Fig. 1. Maps of (a) Japan, (b) the Sanriku Coast and (c) Otsuchi Bay, and (d, e) schematic diagrams of domains used in (d) the Otsuchi Bay case (Run#1) and (e) idealized slope domains (Run#2–Run#6). Four lines shown in panel (c) are observational transects for Fig. 4a–d.

model is required to fully resolve internal wave breaking processes, achieving this resolution is computationally expensive. For this reason, Arthur and Fringer (2014, 2016) showed that a two-dimensional model generally captures internal wave breaking dynamics and cross-shore mass transport when compared to a similar three-dimensional model. In order to limit computational expense in the present study, we assume that our two-dimensional model is appropriate to reproduce internal wave breaking dynamics and cross-shore mass transport.

The sediment resuspension model used in this study was developed by Scheu (2016). The transport equation for suspended sediment in the model is given by

$$\frac{\partial C}{\partial t}+\nabla\cdot(\mathbf{u}C)-\frac{\partial}{\partial z}(w_S C)=\nabla_H(\kappa_H\nabla_H C)+\frac{\partial}{\partial z}\left(\kappa_V\frac{\partial C}{\partial z}\right), \tag{5}$$

where C is the suspended sediment concentration and w_S is the settling velocity. The particle settling velocity, w_S, for small particles sizes can be determined with the Stokes' formula

$$w_s=\frac{(\rho_s-\rho_0)gD^2}{18\mu} \tag{6}$$

where ρ_s is the density of particles, D is the particle diameter and μ is the dynamic viscosity of water. The sediment erosion rate from the bed into the bottom cell, E_b, is represented as

$$E_b=E_0\ \exp\left(\alpha\Delta\tau_b^{\beta}\right) \tag{7}$$

where E_0 is the erodibility, a and β are empirical constants, and $\Delta\tau_b$ is the excessive shear stress described as

$$\Delta\tau_b=\tau_b-\tau_{cr} \tag{8}$$

where τ_b is the bed shear stress and τ_{cr} is the critical shear stress for erosion. Sediment resuspension occur only when $\Delta\tau_b$ exceeds 0. The bed shear stress is computed from the following formula

$$\tau_b=\rho C_D U^2, \tag{9}$$

where C_D is the drag coefficient and U is the velocity magnitude at the bottom cell. The drag coefficient can be written as follows using the log law

$$C_D=\left(\frac{k}{\log(z/z_0)}\right)^2 \tag{10}$$

where $k=0.41$ is the von Kármán constant and z_0 is the bed roughness coefficient. The critical shear stress and the bottom roughness are set to 0.03 N m^{-2} and 5×10^{-5} m respectively, which are reasonable values for a bed composed primarily of silts (Soulsby, 1997). Numerical paramaters used in the model are listed in Table 1.

Table 1
Numerical parameters used in the model.

Parameter	Value	Name of the parameter
z_0	5×10^{-5} m	Bed roughness
τ_C	0.03 N m^{-2}	Critical shear stress
ρ_S		2650 kg m^{-3}
Particle density		
E_0	0.1	Erodibility
α	4.5	Empirical constant α
β	1	Empirical constant β

2.2. Numerical grid and initial condition

We use realistic topography representing Otsuchi Bay, Japan, as well as six idealized topographies (Fig.1, Table 2). Otsuchi Bay is located along the Sanriku Coast, Japan, and is known to produce highly-nonlinear internal bores during the summer (e.g., Masunaga et al., 2015). Recent studies have also demonstrated sediment resuspension processes associated with internal bores in the bay (Masunaga et al., 2015; Masunaga et al., 2016). The bathymetric slope, dz/dx, for the Otsuchi Bay domain (Run#1) was set at 0.012 for the gradual slope (depth 0–40 m) and 0.0066 for the steep slope (depth 40–80 m). The bottom in the bay consists of fine sediment, a mixture of silts and sands with a median particle size of approximately 0.1 mm at 20 m depth (Masunaga et al., 2015). The viscous sublayer thickness is generally of the order of 1 mm on the sea floor (Caldwell and Chriss, 1979), which is larger than the size of sediments in Otsuchi Bay. In addition, the viscous layer thickness estimated with $\delta=\sqrt{2\nu(L/c)}$, where ν is the kinematic viscosity, L is the wave length and c is the wave propagation speed (Arthur and Fringer, 2014). For internal bores in Otsuchi Bay, $L=O(10\ m)$ is the length of the vortex core due to internal bores and $c=O(0.1\ \text{m s}^{-1})$, giving $\delta=O(10\ \text{mm})$. Thus, the bottom of the bay can be considered hydraulically smooth. We also consider five idealized cases with uniform slopes that range from 0.005 to 0.04 (Run#2–Run#6). The domains used for Run#1–Run#6 (both realistic and idealized slopes) include 10 km of flat topography offshore of the slope with a maximum depth of 80 m (Fig. 1d,e). We also run the model with a no-slope condition in order to investigate physical processes without internal wave breaking (Run#7). The left boundary is open for the no-slope case such that waves do not reflect off of the boundary. The numerical setup follows Masunaga et al. (2015). For all cases, the horizontal and vertical grid spacing are 20 m and 0.56 m, respectively, and are constant throughout the domain. To maintain model stability based on the Courant condition related to explicit calculation of internal gravity waves, the time step is set to 1 s. Lastly, to investigate the sensitivity of model results to eddy coefficients, we run the model with constant eddy coefficients that are smaller to those calculated by the MY2.5 turbulence closure scheme for Run#1 (see details in Appendix A).

In order to reproduce internal tides in the model, the offshore boundary is forced by a first-mode internal wave with M_2 semidiurnal frequency. The velocity amplitude of the internal wave at the boundary, U_0, is shown in Table 2. In this study, we consider only internal wave forcing in order to isolate its effect on sediment resuspension and transport from other forcing mechanisms that are present in the field. Furthermore, we do not employ a heat flux model at the sea surface since the time scale of the simulations is not long enough to be influenced by thermally-driven circulation. Initial temperature and salinity are constant in the horizontal and are initialized in the vertical with typical temperature and salinity conditions from a field survey in Otsuchi Bay on September 11, 2013 (Masunaga et al., 2015). For all cases, the

Table 2
Physical parameters used in the numerical simulations, including the density difference between the upper and lower layers ($\Delta\rho$), the velocity amplitude of internal wave forcing (U_0), the mode-1 internal wave speed at the boundary (C_1), the wave amplitude at the boundary (a), the wave length (λ), the topographic slope (s) and the internal Iribarren number (ξ).

Run	$\Delta\rho$	U_0 (ms^{-1})	C_1 (ms^{-1})	a	λ (km)	s	ξ
Run#1 (Otsuchi Bay)	2.2	0.20	0.66	6.0	30	0.012–0.0066	0.47–0.85
Run#2	2.2	0.15	0.66	4.5	30	0.04	3.2
Run#3	2.2	0.15	0.66	4.5	30	0.02	1.6
Run#4	2.2	0.15	0.66	4.5	30	0.013	1.1
Run#5	2.2	0.15	0.66	4.5	30	0.008	0.65
Run#6	2.2	0.15	0.66	4.5	30	0.005	0.41
Run#7	2.2	0.20	0.66	6.0	30	0.0	0.0

sediment particle diameter is set to 10 μm (fine silt). Because the sediment in Ostuchi Bay is known to consist of a mixture of silts and sands (Masunaga et al., 2015), an additional particle diameter of 50 μm is included in the Otsuchi Bay case (Run#1). The initial sediment concentration in the water column is set to zero and sediments are initialized only on the sloping bottom (Fig.1, distance < 10 km), not on the flat offshore bottom.

The internal Iribarren number (Boegman et al., 2005) has been used in previous studies to analyze breaking internal waves on slopes and is represented by

$$\xi = \frac{s}{\sqrt{\frac{a}{\lambda}}}, \tag{11}$$

where s is the topographic slope, a is the internal wave amplitude and λ is the internal wavelength, such that a/λ represents the internal wave steepness. The internal Iribarren number has been used to classify wave breaker types (Boegman et al., 2005; Aghsaee et al., 2010) and to quantify wave reflection (Bourgault and Kelley, 2007; Aghsaee et al., 2010), mixing efficiency (Boegman et al., 2005; Arthur and Fringer, 2014), and particle transport (Arthur and Fringer, 2016). It is known that wave breaking with strong turbulent mixing occurs under low Iribarren number conditions (Boegman et al., 2005; Masunaga et al., 2016). By contrast, under high Iribarren number conditions, the mixing due to wave breaking is weak and much of incoming wave energy reflects back offshore (Masunaga et al., 2016). According to laboratory experiments conducted by Boegman et al. (2005), over a half of incoming wave energy is dissipated when ξ is less than ~0.8. Walter et al. (2012) and Masunaga et al. (2016) reported that canonical bores accompanied by strong turbulent mixing occur in low Iribarren number conditions. In our simulations, ξ ranges between 0.41 and 3.2 (Run#2–#6).

3. Generation of INLs

3.1. Sediment resuspension and INL generation

Numerical results from SUNTANS show the run-up of internal bores along the sloping bathymetry (Fig. 2). During the first run-up phase, the bore head generates weak sediment resuspension at the front of the bore (Fig. 2, periods A, B and C, sediment concentration is too weak to see in the Figure). The shoreward flow speed is approximately 0.2 m s^{-1} in this period. Strong downslope currents appear after the run-up phase, resulting in strong vertical shear (Fig. 2, period D). The flow speed in the downslope flows is much higher than that in the run-up bore, reaching 0.4 m s^{-1}. During the second run-up phase, the bore interacts with the downslope flow from the previous wave (Fig. 2, period E). This interaction causes convergence and upward motion at the bore head, resulting in strong vertical resuspension. The second bore propagates shoreward accompanied by a high concentration of suspended sediments (Fig. 2, periods F and G). In this phase, the cold bore water near the bottom intrudes below the suspended sediments and generates an INL along the interface of the wave. Although sediments with larger grain sizes (50 μm) are suspended during the receding phase and at the head of the bore, these sediments deposit quickly and are not present within the INL (not shown).

Shoreward currents of run-up bores generate a strong upward flow at the front of the bore head (Fig. 3c,d). This upward flow is induced by the convergence of the run-up bore and the downslope flow from the previous wave. The upward flow speed reaches 0.09 ms^{-1} when the bore head is at roughly 40 m depth. A downward flow occurs behind the head of the bore. This phenomenon at the bore head has been termed a "vortex" (Boegman and Ivey, 2009; Masunaga et al., 2015) or "updraft" (Cheriton et al., 2014). Although the spatial scale of the vortex is too small to be captured using conventional oceanographic profiles, recent observational technologies have revealed the structure of the vortex motion due to internal waves (Van Haren, 2009; Masunaga et al., 2015). According to these studies, strong shoreward currents (that exceed the propagation speed of the bore) generate instabilities and highly nonlinear vortex motion at the head of the bore. Fine suspended particles (fine silts or clays) follow the same motion as the vortex, since the flow speed in the vortex is much higher than the settling velocity of the particles. In our simulations, the vortex motion at the bore head lifts suspended sediments up to 10 m above the bottom (Fig. 2, period F and G) and then the suspended sediments intrude offshore, which is consistent with the hypothesis suggested by Cheriton et al. (2014).

According to the numerical results, INLs are generated through the following processes, which are illustrated in Fig. 3:

(1) Downslope flows from a previous shoaling internal wave lead to sediment resuspension on the slope (Fig. 3b).
(2) The interaction of the downslope flows and the next run-up bore induces strong horizontal flow convergence (Fig. 3c).
(3) The upward motion (vortex) due to the convergent flows lifts fine suspended sediments up into the interface of the bore (Fig. 3c).
(4) The cold internal bore intrudes below the suspended sediments, forming an INL along the interface of the internal waves (Fig. 3d).

3.2. Comparison of model and field results

Numerical results can be compared with observed data from in situ surveys (Masunaga et al., 2015). Observed data were obtained in Otsuchi Bay on September 11, 2013 using a tow-yo CTD instrument, the YODA Profiler (Masunaga and Yamazaki, 2014). Turbidity from the YODA Profiler is detected by the optical backscatter sensor. Internal bores accompanied by INLs intermittently appeared in the bay during the summer season. However, it is difficult to capture clear bore structures from field surveys because their arrivals are not correlated with sea-surface tidal elevations. Although we carried out numerous field surveys in the bay, the observed results shown in Fig. 4 are the best data set for showing sediment resuspension associated with internal bores.

Both the numerical results and the observed data show strong sediment resuspension at the head of the bore and INLs along the pycnocline (Fig. 4). The INL reproduced by the numerical model shows good agreement with the observed data. However, the suspended sediment concentration in the bottom boundary layer in the model appears to be higher than the observed turbidity. A plausible reason for this difference is that the turbidity data from the optical backscatter sensor includes not only suspended sediment, but also biological particles (e.g., plankton and biological aggregates). Flocculation processes could also lead to higher settling velocities that reduce the turbidity. Other possible reasons include cross-shore differences in suspended sediment concentrations, three-dimensional internal wave motions and background flows in the bay. The strong vertical resuspension induced by the vortex motion at the bore head does not appear in the observed data. This inconsistency is due to the horizontal resolution of the observation; the size of the vortex is much smaller than the horizontal resolution of the YODA Profiler survey (~100 m). In addition, the size of the vortex may be overestimated in the numerical simulation due to the grid resolution. The actual horizontal scale of the vortex should be O(10 m) (Masunaga et al., 2015). However, one observed profile does show vertical resuspension of sediments that were likely induced by the bore head vortex (Fig. 4c, distance ~1 km). Although the numerical model is greatly simplified, the results indicate that the SUNTANS model can qualitatively reproduce the observed sediment resuspension and INLs generated by internal bores.

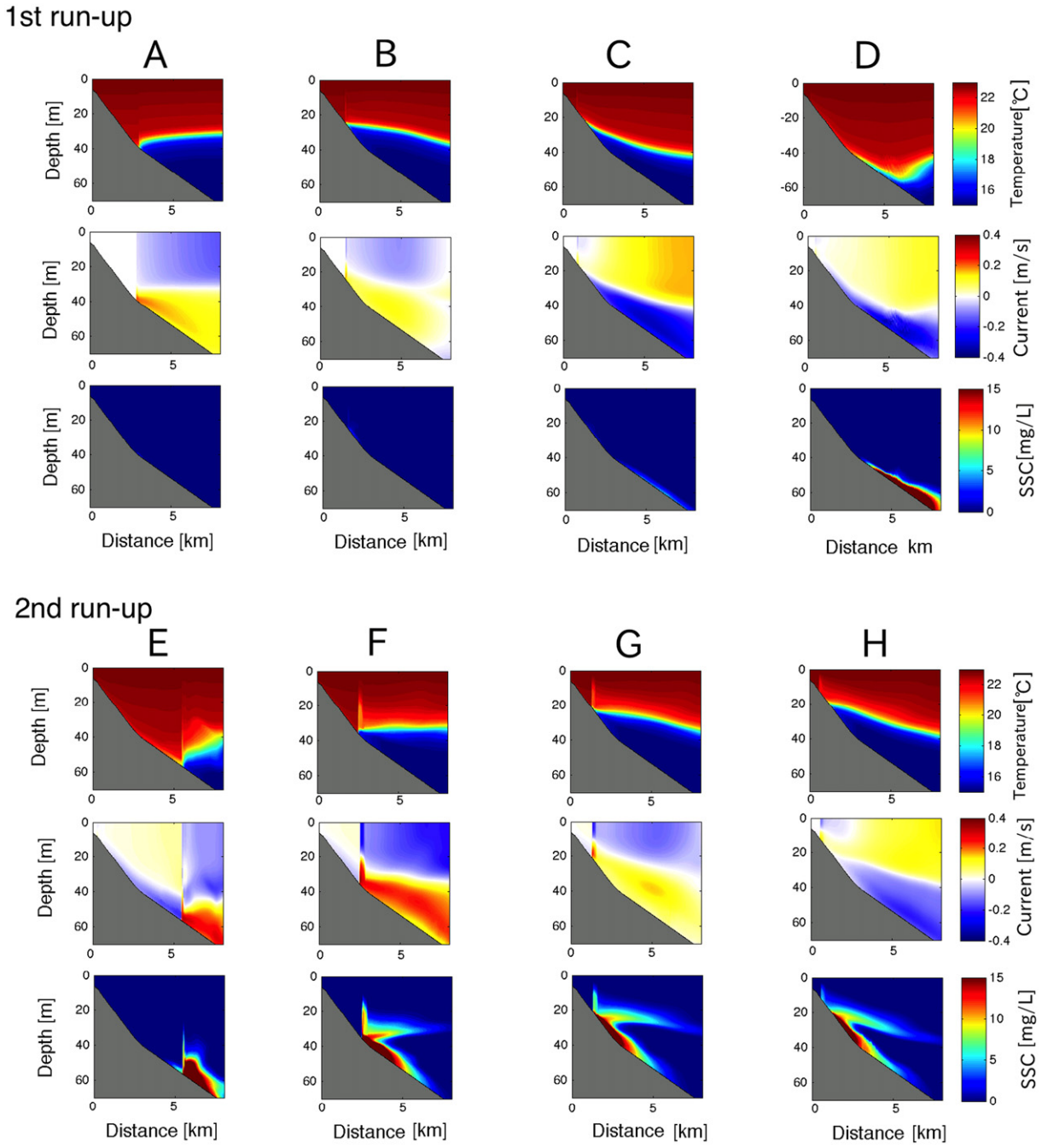

Fig. 2. Numerical results from Otsuchi Bay produced by numerical simulations (Run#1). (A–H) vertical section results for temperature, horizontal current and suspended sediment concentration (SSC) of fine particles (10 μm) [mg L^{-1}]. Panels (A–D) and (E–H) show the first run-up bore and the second run-up bore respectively.

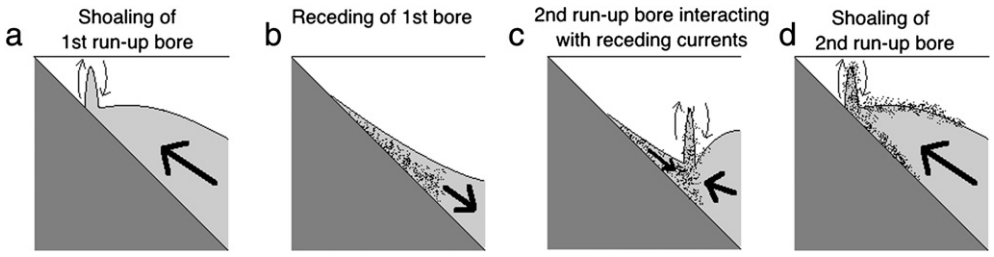

Fig. 3. Schematic image of sediment resuspension induced by internal bores. (a) The 1st run-up bore, (b) the receding of the 1st run-up bore accompanied by sediment resuspension, (c) the interaction of receding currents and the 2nd run-up bore with strong vertical sediment resuspension and (d) the 2nd run-up bore accompanied by intermediate nepheloid layer formation.

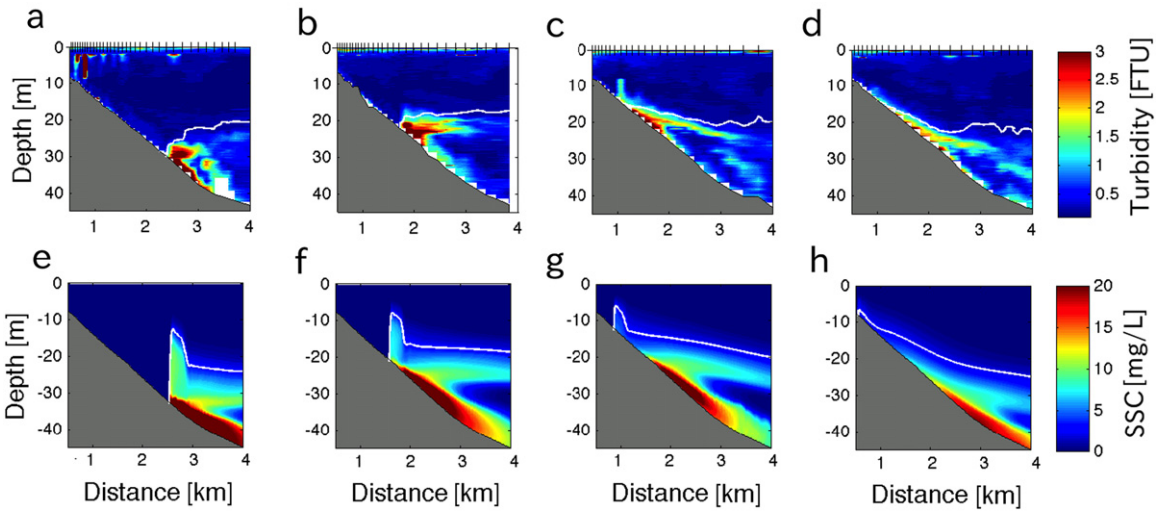

Fig. 4. Comparison between (a–d) observed results of turbidity and (e–h) model results of SSC. White contour lines show isothermal depth of 21 degrees.

3.3. Time evolution of INLs

Intermediate density water on a slope created by locally intensified vertical mixing during wave breaking leads to the development of a horizontal (cross-shore) buoyancy gradient. This gradient drives the transport of mixed intermediate density water offshore, often referred to as convergent flow or tertiary circulation. It is known that this convergent flow transports material from the sloping bottom to the interior of the water column offshore (Garrett, 1990). Enhanced mixing over the slope (distance = 2–6 km) is evident in Fig. 5c, which shows the maximum eddy diffusivity as a function of cross-shore distance. The eddy diffusivity reaches 10^{-1} m^2 s^{-1} on the slope and is 10^3 times larger than that in the offshore flat region. As suggested by studies of tertiary circulation, our numerical results indicate growth of the INL over the course of successive internal bore events (Fig. 5b). Numerical results during the fifth bore phase, when the INL reached approximately 10 km offshore from the sloping bottom, are shown in Fig. 5a. Simulated time series show the growth of the INL along the pycnocline, which oscillates vertically due to the presence of internal waves (Fig. 6c). The concentration of sediment in the pycnocline increases over time. The horizontal sediment flux (SSC Flux) due to advection was estimated from the horizontal velocity and suspended sediment concentration. The offshore sediment flux within the pycnocline reaches 10 mg L^{-1} m s^{-1} and is much larger than the onshore flux (Fig. 6d), indicating a net offshore sediment flux due to the convergent flow.

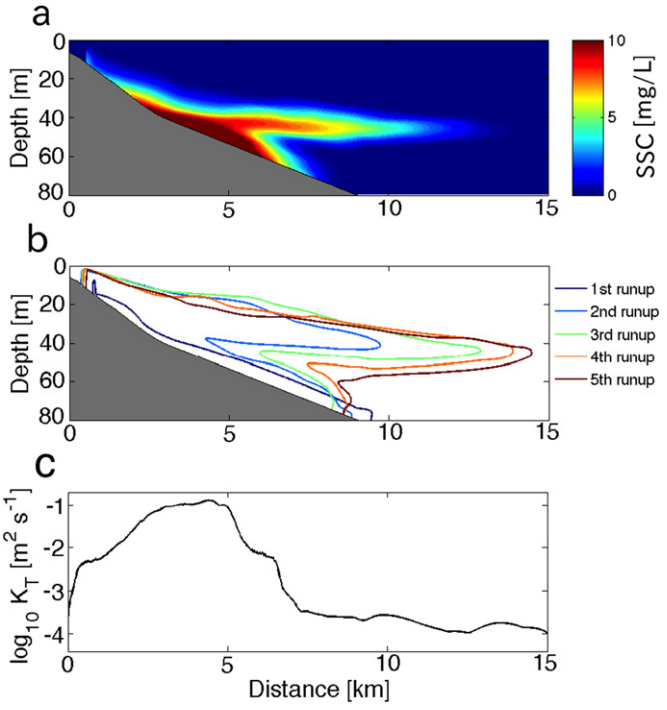

Fig. 5. (a) Suspended sediment distribution during the fifth run-up phase (62.5 h after simulation started), (b) the distribution of INLs (SS = 0.1) in each run-up phase and (c) the maximum vertical eddy diffusivity as a function of distance for Run#1 (Otsuchi Bay case). Thick lines in panel (b) are the outlines of SS = 0.1 mg L in the first (dark blue), second (light blue), third (light green), fourth (orange) and fifth (brown) run-up phases.

The convergent flow generated by breaking internal waves can be seen in the mean profiles taken over a vertical cross section at the 80 m isobath (Fig. 6f,g). The mean quantities in Fig. 6f are computed between the third and fifth wave period, and are plotted as a function of the initial isothermal depth. The mean current speed (Fig. 6f) indicates an offshore flow in the middle layer (interface of waves, depth ~ 40 m) and shoreward flow in the lower (depth > 48 m) and the upper (depth < 25 m) layers. The peak of the mean flow occurs at the interface of the wave (40 m depth), reaching 0.05 m s^{-1}. The offshore current at the wave interface leads to an offshore sediment flux (Fig. 6e) that is generated by the convergent flow due to bottom boundary mixing. Since the convergent flow is much greater than the sediment settling velocity, sediment particles are essentially transported offshore as passive tracers. If the model domain was large enough and the simulation was run for a long enough time, suspended sediment particles would eventually settle to the bottom far from the breaking wave site. If particles are transported offshore with a constant speed due to the convergent flow (0.05 m s^{-1}) and with a constant sinking velocity given by Eq. (6), they are deposited approximately 24 km from the slope within 5.6 days (134 h).

The vertically integrated offshore flux due to the convergent flows was estimated as 0.74 m^2 s^{-1} for the Otsuchi Bay case (Run#1, Fig. 6). Although the numerical model was two dimensional, a total outflow flux caused by the convergent flows can be estimated using the approximate width of the bay mouth. Assuming a width of 3000 m, the total outflow flux due to the INLs is 2.2×10^3 m^3 s^{-1}, which is much greater than the total river discharge flowing into Otsuchi Bay (on the order of 10 m^3 s^{-1}).

In addition to the convergent flow driven by internal wave breaking on the slope, it is known that nonlinear internal waves without wave breaking on a flat bottom (in the absence of a slope) also transport

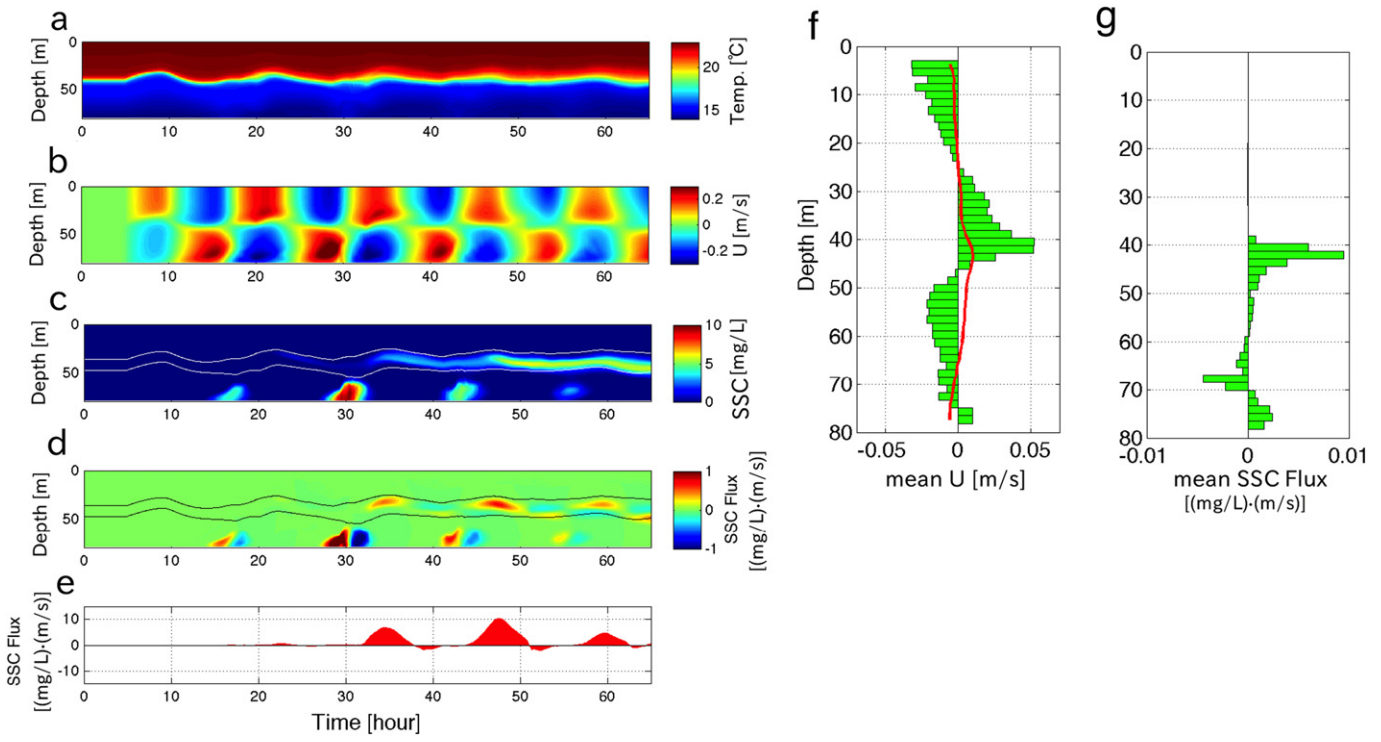

Fig. 6. Time series of numerical results at 80 m depth for Run#1 (the bottom edge of the slope). (a) Temperature, (b) horizontal current, (c) suspended sediment concentration [mg L^{-1}], (d) flux of suspended sediments and (e) integrated flux of suspended sediments in the interface of the bore wave (temperature between 16.5 and 22.6 °C). (f) Mean current speed and (g) mean sediment flux. Contour lines in panels (c) and (d) are isothermal depths of 16.5 and 22.6 °C. A positive (negative) value in panels (b, d, e, f and g) indicates an offshore(onshore) current or flux. The red line in panel (f) is mean current profile due to Stokes drift from Run#7.

mass (Lamb, 1997; Arthur and Fringer, 2016). Such transport by nonbreaking internal waves increases with increasing wave amplitude (Lamb, 1997). Internal-wave Stokes drift must also be considered when investigating mass transport in the ocean (e.g., Thorpe, 1968; Wunsch, 1971). We therefore run the model without the slope (Run#7) to investigate water mass fluxes in the absence of wave breaking. For the no-slope case (Run#7), all parameters are the same as those in the Ostuchi Bay case (Run#1). The mean current for the no-slope case shows an offshore flux in the middle of the water column (depth 30–60 m) and onshore fluxes in the lower and upper layers (Fig. 6f red line). This mean profile is similar to the internal wave Stokes drift velocity profile suggested by Thorpe (1968). However, the offshore flux for the no-slope case is <0.01 m s^{-1}, much less than the convergent flow induced by bottom boundary mixing during wave breaking on a slope (Fig. 6f). Therefore, we conclude that the offshore flux over the slope is dominated by the convergent flow induced by bottom boundary mixing on the slope during wave breaking as opposed to non-breaking effects. The generation process of INLs shown in this study is therefore consistent with the laboratory-scale numerical experiment conducted by Arthur and Fringer (2016).

4. Topography and sediment resuspension

We investigate the effect of topography on sediment resuspension and the formation of INLs during breaking internal wave events using the results of several idealized simulations with uniform bathymetric slopes (Run#2–Run#6, Table2). We classify these simulations using the internal Iribarren number, which is defined in Eq. (12). Numerical results show two general types of internal bores:

(1) Bores with a sharp drop in bottom temperature followed by a gradual increase bottom temperature. Such an internal bore has been termed a "canonical bore" (Walter et al., 2012) since nonlinear internal waves typically form this feature (e.g., Alford et al., 2015; Masunaga et al., 2016). This type of internal bore generates strong turbulent mixing induced by the interaction of receding currents from one bore event with the run-up currents of a subsequent bore (Masunaga et al., 2016).

(2) Non-canonical bores drive a gradual decrease in bottom temperature followed by a rapid increase in bottom temperature. Walter et al. (2012) observed this type of bore on a steep slope in Monterey Bay, California, and found strong turbulent mixing when the bore recedes offshore. The mixing intensity of this type of bore is weaker than the canonical bores, since the non-canonical bore does not interact with receding bores (Masunaga et al., 2016).

The transition from canonical bores to non-canonical bores is controlled by the internal Iribarren number (Walter et al., 2012; Masunaga et al., 2016). In our simulations, the low Iribarren number cases (e.g., $\xi = 0.45$ in Fig. 7) result in canonical bores and the high

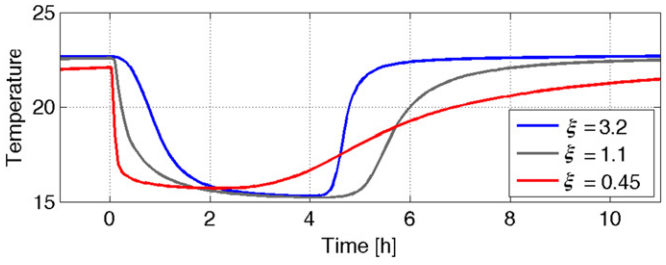

Fig. 7. Bottom temperature time series at 30 m for high (blue), intermediate (grey) and low (red) ξ conditions.

Iribarren number cases (e.g., $\xi = 3.2$ in Fig. 7) result in non-canonical bores. Internal bores simulated for the case of $\xi = 1.1$ appear to be in a transition regime between canonical and non-canonical bores (Fig. 7). The magnitude of the up-slope current during the run-up phase increases with a decrease in the Iribarren number (Fig. 9b,e,h,k,n), resulting in strong currents and vortex motion at the head of the bores for the low ξ cases. Internal bores on gentle slopes have to run-up longer distances than those on steep slopes; therefore, gentle slope conditions (low ξ) cause strong horizontal currents in bores leading to highly non-linear motion.

The two low Iribarren number cases (Run#5 and 6, $\xi = 0.65$ and 0.45) produce strong sediment resuspension and INLs (Figs. 8l,o and 9f,g). The internal bore for the intermediate ξ case (Run#4, $\xi = 1.1$) suspends sediments around the bore head vortex, but the bore does not generate a visible INL (Figs. 8i and 9h). Strictly speaking, the case of $\xi = 1.1$ produces a weak INL, although the associated sediment concentration is 10 times smaller than that for the $\xi = 0.65$ and 0.45 cases. Results from the $\xi = 1.6$ case show weak sediment resuspension only during the receding phase (Fig. 8f). The maximum bottom shear stress significantly exceeds the critical shear stress for the $\xi = 1.1$ and 1.6 cases (Fig. 9m,n). These two cases do not show strong vertical sediment resuspension and INLs, because run-up bores do not interact with receding flows resulting in strong upward flows. The highest ξ (3.2) case does not produce any sediment resuspension, and therefore no INL (Figs. 8c and. 9j), because the bottom shear stress does not reach the critical stress for resuspension (Fig. 9o). For long internal waves propagating up a uniform slope, the numerical results of Runs#2–#6 indicate that sediment resuspension and subsequent INL formation are limited to low Iribarren number conditions. In addition, the bottom shear stress is not the only factor that controls sediment resuspension and INL formation during breaking internal wave events. The strong upward motion arising from the interaction of receding currents and subsequent run-up bores plays a significant role in the sediment resuspension processes.

5. Summary and discussion

Numerical simulations performed with the SUNTANS model reproduced sediment resuspension and intermediate nepheloid layers (INLs) induced by internal bores. Downslope receding currents due to a previous wave caused strong bottom shear stress leading to sediment resuspension. Strong upward motion was generated by the interaction of the receding currents and a subsequent run-up bore, lifting suspended sediments into the interior of the water column. The run-up bore intruded below the resuspended sediments and generated an INL. Internal bores enhanced turbulent mixing near the sloping bottom, leading to convergent flows (tertiary circulation). The convergent flows transported sediments offshore within the INL. In the Otsuchi Bay simulation case (Run#1), the mean offshore flow speed caused by the convergent flow was approximately 0.05 ms^{-1} within the pycnocline. Cases with various internal Iribarren numbers showed that strong sediment resuspension and INLs are induced by canonical bores in low internal Iribarren number conditions ($\xi = 0.41$ and 0.65).

Several studies have used the results of numerical simulations to report mass or sediment transport and the generation of INLs by breaking internal waves (e.g., Bourgault et al., 2014; Arthur and Fringer, 2016). Bourgault et al. (2014) employed a two-dimensional numerical simulation to investigate field-scale sediment resuspension and INLs induced by internal solitary waves on a gentle slope. They showed details of internal solitary wave breaking accompanied by sediment resuspension and INL formation. Arthur and Fringer (2016) conducted laboratory-scale direct numerical simulations with a Lagrangian particle-tracking model (without settling velocity), and related the entrainment of particles into the INL to turbulent mixing driven by wave breaking.

A major difference between the present study and previous works is the type of internal waves. Both Bourgault et al. (2014) and Arthur and Fringer (2016) investigated sediment or mass transport caused by one or two internal solitary waves. The wavelength of the field-scale internal solitary waves investigated by Bourgault et al. (2014) was on the

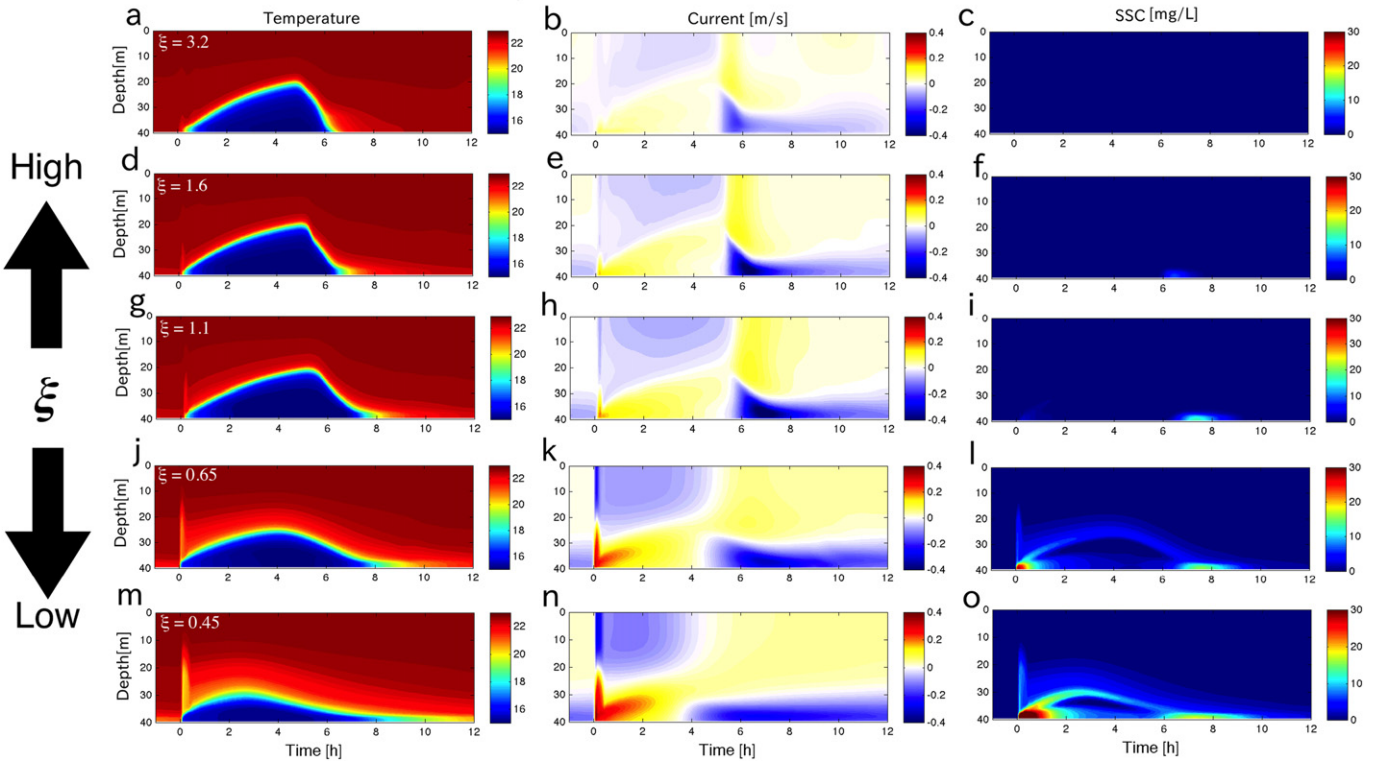

Fig. 8. Time series data at 40 m depth during second wave run-ups simulated in five-slope cases, (a–c) $\xi = 3.2$ (Run#2), (d–f) $\xi = 1.6$ (Run#3), (g–h) $\xi = 1.1$ (Run#4), (j–l) $\xi = 0.65$ (Run#5) and (m–o) $\xi = 0.45$ (Run#6). Left panels are temperature, middle panels are horizontal current [m s^{-1}] and right panels are suspended sediments [mg L^{-1}].

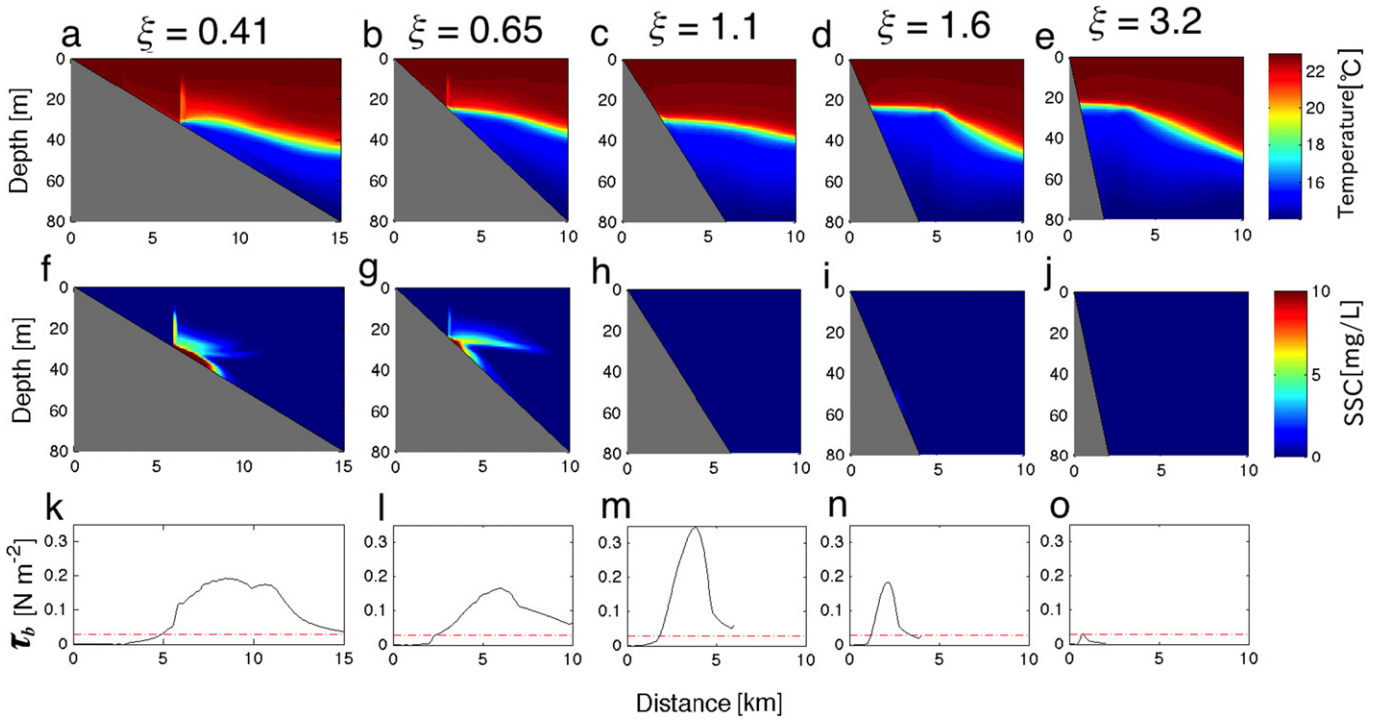

Fig. 9. (a–e) Temperature, (f–j) the concentration of suspended sediments during the 2nd run-up and (k–o) the maximum bottom shear stress on the slope for five Iribarren number conditions. Red dashed lines in bottom panels (k–o) show the critical shear stress, 0.03 N m^{-2}, for sediment resuspension in the model.

order of 100 m and the time scale of the breaking event was 1 h. In our study, we investigated periodic internal tides that produce repeated internal tidal bores with a horizontal wavelength of 30 km and a time scale of the M_2 tidal period (12.42 h). Thus, the scale of the waves studied here is much larger than the internal solitary waves studied previously. Despite these differences, there are some important similarities between our results and those of previous studies: (1) the vortex structure, or upward flows, that lift sediments up and (2) the growth of INLs related to mixing intensity and the Iribarren number. While our results are consistent with those in previous studies, we have found two new important processes causing sediment resuspension and INLs for large-scale internal bores: sediment resuspension due to (1) receding bores and (2) the interaction of successive bores. These phenomena likely only occur for large-scale internal tidal bores under low Iribarren number conditions.

The vortex motion generated by internal waves is known as an important phenomenon for sediment resuspension and mass transport (e.g., Van Haren, 2009; Stastna and Lamb, 2002; Bourgault et al., 2014; Masunaga et al., 2015, Arthur and Fringer, 2016). As internal waves shoal and break, they form a vortex with strong vertical currents that lift sediments up from the bottom. In field surveys, Van Haren (2009) reported a large vortex structure accompanied by suspended sediment with a height of roughly 40 m. Field measurements conducted by Cheriton et al. (2014) suggested that the updraft motion generated by internal bores suspends sediment resulting in INLs. Masunaga et al. (2015) observed the vortex motion generated by shoaling internal bores, which results in strong sediment resuspension and INLs. In addition to field surveys, numerical simulations have revealed details of the vortex motion generated by shoaling internal bores (e.g., Stastna and Lamb, 2002; Bourgault et al., 2014; Arthur and Fringer, 2016). Despite the differences in the scale of the internal tidal waves studied here with the solitary waves in previous studies, the vortex dynamics appear to be similar. The horizontal scale of the vortex at the head of internal tidal bores is $O(10\ \mathrm{m})$, which is consistent with the size of the vortex generated by field scale internal solitary waves in previous studies (Bourgault et al., 2014). Thus, it is clear that vortex motion plays a significant role in sediment resuspension processes both for small-scale internal solitary waves and field-scale internal tidal bores.

Once sediments are suspended into the water column, they are transported by mean flows. On the sloping bottom, the convergent flow induced by boundary mixing is known as one of the major contributors to transport suspended sediment into the offshore water column (Garrett, 1990). A horizontal buoyancy gradient due to boundary mixing generates this convergent flow, which results in INLs (see details in Section 3.3 *Time evolution of INLs*). The strength of the convergent flow increases with an increase in the mixing intensity on the slope because vertical mixing drives the horizontal density gradient. It is well known that the mixing intensity due to internal wave breaking increases with a decrease in the internal Iribarren number (e.g., Boegman et al., 2005; Arthur and Fringer, 2016; Masunaga et al., 2016). For example, Arthur and Fringer (2016) showed a clear relationship between the growth of INLs and the internal Iribarren number. Bourgault et al. (2014) also presented a linear relationship between the growth of INLs and incoming wave energy. Ranges of the internal Iribarren number investigated by Arthur and Fringer (2016) and Bourgault et al. (2014) are 0.24–1.51 and 0.04–1.28, respectively, which are similar to the range studied here (Table 2, $\xi = 0.41$–3.2). Our numerical results also showed strong boundary mixing by internal wave breaking and enhanced sediment resuspension in low internal Iribarren number conditions.

Internal wave breaking is not the only mechanism capable of resuspending sediment on the continental shelf. In fact, surface gravity waves are thought to be the predominant contributor to sediment resuspension on the shelf (Sternberg and Larsen, 1975; George and Hill, 2008). It is well known that the bottom stress induced by surface waves frequently reach the critical shear stress in shallow coastal regions (Soulsby, 1997). Noble and Xu (2003) reported that the bed shear stress due to surface gravity waves dominates resuspension processes and is more important than tidal flows at a site with a depth of 35 m. Cheriton et al. (2014) showed the critical shear stress induced by the superposition of tidal currents and surface waves. However, the orbital velocity caused by surface waves may not generally lift

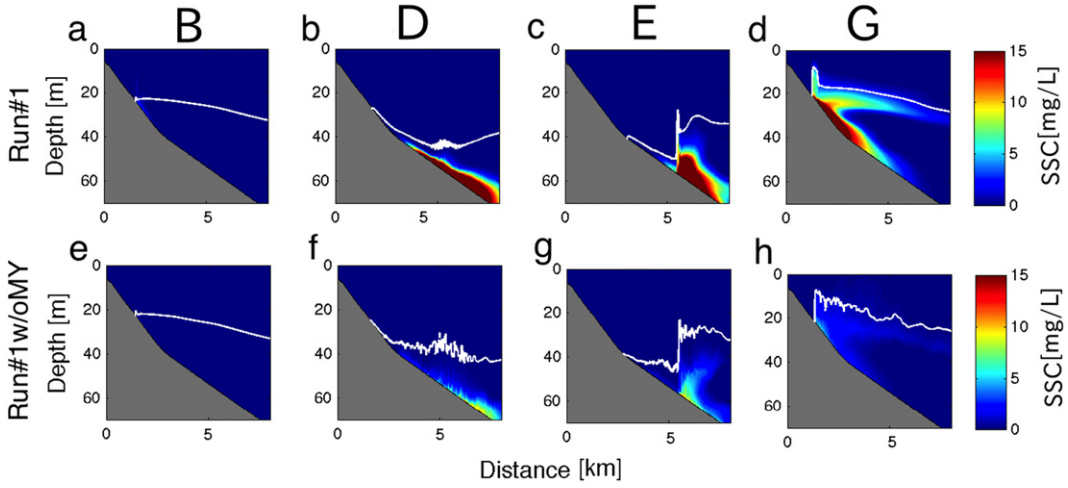

Fig. A1. Suspended sediment concentrations from (a–d) Run#1 (e–h) Run#1w/oMY. White contour lines show isothermal depth of 21 degrees. Periods of B, D, E and G are consistent with those in Fig. 2.

sediments up into the water column and cause INLs, except in extreme weather conditions.

In addition to surface gravity waves, background flows such as geostrophic flows can also increase the bottom shear stress. Sediment resuspension and INL formation caused by geostrophic flows were observed by Puig and Palanques (1998) along a deep slope. However, the velocity of geostrophic currents is generally small near the coast and these flows are therefore not expected to suspend sediment in coastal regions. Thus, the formation of INLs in coastal regions is likely dominated by internal waves.

Internal waves and INLs have been observed in coastal oceans worldwide and are known as important phenomena for maintaining ocean ecosystems. As demonstrated in this study, canonical internal bores generate sediment resuspension and can facilitate INL formation under low internal Iribarren number conditions. Such canonical bores with sharp leading wave fronts have been observed frequently in coastal oceans (Thorpe, 1998; Leichter et al., 1996; McPhee-Shaw et al., 2004, Masunaga et al., 2016) and likely contribute to extensive offshore sediment fluxes. This study suggests that the offshore sediment flux in INLs might be predicted using internal Iribarren number.

Acknowledgements

We are indebted to the laboratory members of LOCEANED (Tokyo University of Marine Science and Technology) for obtaining filed survey data in Otsuchi Bay. This study was supported by funding from Tohoku Ecosystem-Associated Marine Sciences (TEAMS), a research program launched by the Ministry of Education, Culture, Sports, Science and Technology (MEXT). RSA and OBF acknowledge ONR grant N00014-15-1-2287. The authors wish to express sincere appreciation to Captains of M. Kurosawa and M. Hirano for their dedicated works to our field surveys.

Appendix A*Test case with constant eddy coefficients*

In order to investigate sensitivity to the eddy coefficients, Run#1 was run with constant reduced eddy coefficients without the Mellor and Yamada level 2.5 turbulence closure model (MY2.5). The horizontal and vertical eddy-viscosities were set to 10^{-2} and 10^{-4} m^2 s^{-1}, respectively, and the eddy-diffusivities in both the horizontal and vertical directions were set to 0 m^2 s^{-1}. This additional run is referred to as Run#1w/oMY. Numerical results with constant eddy coefficients (Run#1w/oMY) are compared to results from Run#1 with the Mellor and Yamada level 2.5 turbulent closure scheme (Fig. A1). The interface of internal bores shows small-scale and high-frequency motions around the head of the bore, likely a result of reduced mixing because of the smaller eddy coefficients (Fig. 7f,g,h). Sediment resuspension during the receding phase (period D) was reduced for Run#1w/oMY when compared to Run#1. Consequently, the sediment concentration in the INL for Run#1w/oMY was approximately five times smaller than that of Run#1. Therefore, increased eddy-diffusivities due to the turbulence closure scheme contribute to the high concentration of suspended sediment caused by run-up bores. The numerical run for Run#1 without MY2.5 was continued for several tidal periods, however, unrealistic numerical instabilities appeared after the third run-up event. In order to run the model with reasonable eddy coefficients and ensure model stability, the MY2.5 turbulence closure scheme is an appropriate choice for our numerical simulations ($\Delta x = 20$, $\Delta z = 0.56$).

References

Aghsaee, P., Boegman, L., Lamb, K.G., 2010. Breaking of shoaling internal solitary waves. J. Fluid Mech. 659, 289–317.
Alford, M.H., et al., 2015. The formation and fate of internal waves in the South China Sea. Nature 521, 65–69.
Arthur, R.S., Fringer, O.B., 2014. The dynamics of breaking internal solitary waves on slopes. J. Fluid Mech. 761, 360–398.
Arthur, R.S., Fringer, O.B., 2016. Transport by breaking internal waves on slopes. J. Fluid Mech. 789, 93–126.
Boegman, L., Ivey, G.N., 2009. Flow separation and resuspension beneath shoaling nonlinear internal waves. J. Geophys. Res. Oceans 114, C02018.
Boegman, L., Ivey, G.N., Imberger, J., 2005. The degeneration of internal waves in lakes with sloping topography. Limnol. Oceanogr. 50 (5), 1620–1637.
Bourgault, D., Kelley, D.E., 2007. On the reflectance of uniform slopes for normally incident interfacial solitary waves. J. Phys. Oceanogr. 37 (5), 1156–1162.
Bourgault, D., Morsilli, M., Richards, C., Neumeier, U., Kelley, D.E., 2014. Sediment resuspension and nepheloid layers induced by long internal solitary waves shoaling orthogonally on uniform slopes. Cont. Shelf Res. 72, 21–33.
Bruland, K.W., Rue, E.L., Smith, G.J., 2001. Iron and macronutrients in California coastal upwelling regimes: implications for diatom blooms. Limnol. Oceanogr. 46 (7), 1661–1674.
Cacchione, D.A., Pratson, L.F., Ogston, A.S., 2002. The shaping of continental slopes by internal tides. Science 296, 724–727.
Caldwell, D.R., Chriss, T.M., 1979. The viscous sublayer at the sea floor. Science 205, 1131–1132.
Cheriton, O.M., McPhee-Shaw, E.E., Shaw, W.J., Stanton, T.P., Bellingham, J.G., Storlazzi, C.D., 2014. Suspended particulate layers and internal waves over the southern Monterey Bay continental shelf: an important control on shelf mud belts? J. Geophys. Res. Oceans 119 (1), 428–444.
Fringer, O.B., Gerritsen, M., Street, R.L., 2006. An unstructured-grid, finite-volume, nonhydrostatic, parallel coastal ocean simulator. Ocean Model 14, 139–173.
Garrett, C., 1990. The role of secondary circulation in boundary mixing. J. Geophys. Res. 95 (C3), 3181–3188.
Garrett, C., 1991. Marginal mixing theories. Atmosphere-Ocean 29, 313–339.
George, D.A., Hill, P.A., 2008. Wave climate, sediment supply and the depth of the sand-mud transition: a global survey. Mar. Geol. 254, 121–128.
Helfrich, K.R., 1992. Internal solitary wave breaking and run-up on a uniform slope. J. Fluid Mech. 243, 133–154.

Lamb, K.G., 1997. Particle transport by nonbreaking, solitary internal waves. J. Geophys. Res. 102 (C8), 18641–18660.
Leichter, J.J., Wing, S.R., Miller, S.L., Denny, M.W., 1996. Pulsed delivery of subthermocline water to Conch Reef (Florida Keys) by internal tidal bores. Limnol. Oceanogr. 41 (7), 1490–1501.
Masunaga, E., Yamazaki, H., 2014. A new tow-yo instrument to observe high-resolution coastal phenomena. J. Mar. Syst. 129, 425–436.
Masunaga, E., Homma, H., Yamazaki, H., Fringer, O.B., Nagai, T., Kitade, Y., Okayasu, A., 2015. Mixing and sediment resuspension associated with internal bores in a shallow bay. Cont. Shelf Res. http://dx.doi.org/10.1016/j.csr.2015.09.022.
Masunaga, E., Fringer, O.B., Yamazaki, H., Amakasu, K., 2016. Strong turbulent mixing induced by internal bores interacting with internal tide-driven vertically-sheared flow. Gephys. Res. Lett. http://dx.doi.org/10.1002/2016GL067812.
McPhee-Shaw, E., 2006. Boundary–interior exchange: reviewing the idea that internal-wave mixing enhances lateral dispersal near continental margins. Deep-Sea Res. II Top. Stud. Oceanogr. 53 (1), 42–59.
McPhee-Shaw, E.E., Sternberg, R.W., Mullenbach, B., Ogston, A.S., 2004. Observations of intermediate nepheloid layers on the northern California margin. Cont. Shelf Res. 24, 693–720.
Mellor, G.L., Yamada, T., 1982. Development of a turbulence closure model for geophysical fluid problems. Rev. Geophys. 20 (4), 851–875.
Millero, F.J., Poisson, A., 1981. International one-atmosphere equation of state of seawater. Deep-Sea Res. 28A, 625–629.
Moum, J.N., Caldwell, D.R., Nash, J.D., Gunderson, G.D., 2002. Observations of boundary mixing over the continental slope. J. Phys. Oceanogr. 32 (7), 2113–2130.
Noble, M.A., Xu, J.P., 2003. Observations of large-amplitude cross-shore internal bores near the shelf break, Santa Monica Bay, CA. Mar. Environ. Res. 56 (1), 127–149.
Olsthoorn, J., Stastna, M., 2014. Numerical investigation of internal wave-induced sediment motion: resuspension versus entrainment. Geophys. Res. Lett. 41:2876–2882. http://dx.doi.org/10.1002/2014GL059826.
Phillips, O.M., Shyu, J.H., Salmun, H., 1986. An experiment on boundary mixing: mean circulation and transport rates. J. Fluid Mech. 173, 473–499.
Puig, P., Palanques, A., 1998. Nepheloid structure and hydrographic control on the Barcelona continental margin, northwestern Mediterranean. Mar. Geol. 149 (1), 39–54.
Richards, C., Bourgault, D., Galbraith, P.S., Hay, A., Kelley, D.E., 2013. Measurements of shoaling internal waves and turbulence in an estuary. J. Geophys. Res. Oceans 118 (1), 273–286.
Scheu, K., 2016. Sediment transport due to river plumes in stratified, rotationally-influenced lakes. Dissertation, Stanford University, Ph.D.
Soulsby, R., 1997. Dynamics of Marine Sands: A Manual for Practical Applications (Thomas Telford).
Stastna, M., Lamb, K.G., 2002. Vortex shedding and sediment resuspension associated with the interaction of an internal solitary wave and the bottom boundary layer. Geophys. Res. Lett. 29(11).
Sternberg, R.W.S., Larsen, L.H., 1975. Frequency of sediment movement on the Washington continental shelf: a note. Mar. Geol. 21, M37–M47.
Thorpe, S.A., 1968. On the shape of progressive internal waves. Philos. Trans. R. Soc. A Math. Phys. Eng. Sci. 263 (1145), 563–614.
Thorpe, S.A., 1998. Some dynamical effects of internal waves and the sloping sides of lakes. Physical processes in lakes and oceans 441–460.
Van Gastel, P., Ivey, G.N., Meuleners, M.J., Antenucci, J.P., Fringer, O., 2009. The variability of the large-amplitude internal wave field on the Australian North West Shelf. Cont. Shelf Res. 29 (11), 1373–1383.
Van Haren, H., 2009. Using high sampling-rate ADCP for observing vigorous processes above sloping [deep] ocean bottoms. J. Mar. Syst. 77, 418–427.
Venayagamoorthy, S.K., Fringer, O.B., 2006. Numerical simulations of the interaction of internal waves with a shelf break. Phys. Fluids 18:076603/9. http://dx.doi.org/10.1063/1.2221863.
Walter, R.K., Woodson, C.B., Arthur, R.S., Fringer, O.B., Monismith, S.G., 2012. Nearshore internal bores and turbulent mixing in southern Monterey Bay. J. Geophys. Res. Oceans 117 (C7), C07017.
Wunsch, C., 1971. Note on some Reynolds stress effects of internal waves in slopes. Deep-Sea Res. 18, 583–591.